AD-A053 167 AIR FORCE GEOPHYSICS LAB HANSCOM AFB MASS F/G 3/2
HIGH RESOLUTION SOLAR RADIO ACTIVITY INVESTIGATIONS.(U)
NOV 77 R M STRAKA
UNCLASSIFIED AFGL-TR-77-0247 NL

| OF |
AD
A053167

END
DATE
FILMED
5-78
DDC

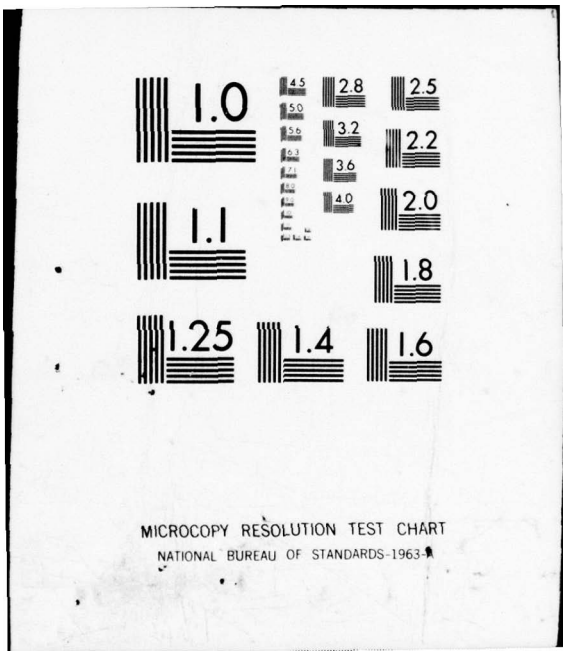
1.0
1.1
1.25
1.4
1.6
1.8
2.0
2.2
2.5
2.8
3.2
3.6
4.0
4.5
5.0
5.6
6.3
MICROCOPY RESOLUTION TEST CHART
NATIONAL BUREAU OF STANDARDS-1963-A

AFGL-TR-77-0247
ENVIRONMENTAL RESEARCH PAPERS, NO. 613

12

High Resolution Solar Radio Activity Investigations

RONALD M. STRAKA

8 November 1977

SPACE PHYSICS DIVISION PROJECT 4643
AIR FORCE GEOPHYSICS LABORATORY
HANSCOM AFB, MASSACHUSETTS 01731

AIR FORCE SYSTEMS COMMAND, USAF

This report has been reviewed by the ESD Information Office (OI) and is releasable to the National Technical Information Service (NTIS).

This technical report has been reviewed and is approved for publication.

FOR THE COMMANDER

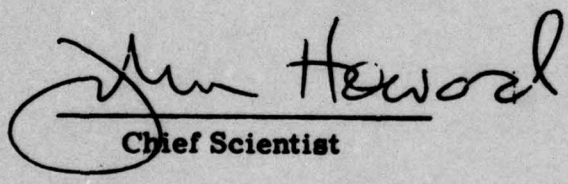

Chief Scientist

Qualified requestors may obtain additional copies from the Defense Documentation Center. All others should apply to the National Technical Information Service.

Unclassified

SECURITY CLASSIFICATION OF THIS PAGE (When Data Entered)

REPORT DOCUMENTATION PAGE

READ INSTRUCTIONS BEFORE COMPLETING FORM

1. REPORT NUMBER: AFGL-TR-77-0247
2. GOVT ACCESSION NO.: (9) Environmental Research papers
3. RECIPIENT'S CATALOG NUMBER:
4. TITLE (and Subtitle): (6) HIGH RESOLUTION SOLAR RADIO ACTIVITY INVESTIGATIONS
5. TYPE OF REPORT & PERIOD COVERED: Scientific, Interim.
6. PERFORMING ORG. REPORT NUMBER: ERP No. 613
7. AUTHOR(s): (10) Ronald M. Straka
8. CONTRACT OR GRANT NUMBER(s):
9. PERFORMING ORGANIZATION NAME AND ADDRESS: Air Force Geophysics Laboratory (PH), Hanscom AFB, Massachusetts 01731
10. PROGRAM ELEMENT, PROJECT, TASK AREA & WORK UNIT NUMBERS: 62101F (17) 03; (16) 46430302
11. CONTROLLING OFFICE NAME AND ADDRESS: Air Force Geophysics Laboratory (PH), Hanscom AFB, Massachusetts 01731
12. REPORT DATE: (11) 8 November 1977
13. NUMBER OF PAGES: (12) 44 p.
14. MONITORING AGENCY NAME & ADDRESS (if different from Controlling Office):
15. SECURITY CLASS. (of this report): Unclassified
15a. DECLASSIFICATION/DOWNGRADING SCHEDULE:

16. DISTRIBUTION STATEMENT (of this Report)

Approved for public release; distribution unlimited.

17. DISTRIBUTION STATEMENT (of the abstract entered in Block 20, if different from Report)

(14) AFGL-TR-77-0247; AFGL-ERP-613

18. SUPPLEMENTARY NOTES

19. KEY WORDS (Continue on reverse side if necessary and identify by block number)

Preflare periodicities	Proton flares
Power spectrum analysis	Flare prediction
Active-region spectra	Centimeter wavelength
High-resolution radio	Prediction parameters

20. ABSTRACT (Continue on reverse side if necessary and identify by block number)

The study of cm-mm wavelength radio emission from solar active regions to find flare/proton flare predictors was the task of AFGL's In-House Work Unit 46430302, High Resolution Solar Activity Investigations. Using mapping data from several large radio telescopes, the multi-wavelength active region data was evaluated for significant prediction parameters.

A statistical examination of 681 solar-region measurements obtained at wavelengths of 9.1 cm (Stanford), 8 mm (AFCRL), and 3 mm (Aerospace) from 1968 to 1970 was made and related to 25 proton events. Of the 21

DD FORM 1 JAN 73 1473 EDITION OF 1 NOV 65 IS OBSOLETE

Unclassified

SECURITY CLASSIFICATION OF THIS PAGE (When Data Entered)

409 578

BB

20. (Cont)

different correlation parameters evaluated, the apparent 3-mm flux density, particularly when it exceeded 10 s.f.u., provided the best indication that a region would produce a proton flare.

Results of the 21 August 1975 proton-flare observations using the 120-ft Haystack radiotelescope at 3.8 cm are discussed. The solar region involved had a low, and decreasing, brightness temperature before it flared, and not the polarization variations often seen prior to flares. The noise power spectrum analysis of active-region temperature and polarization variations is described. A significant power component was found at 43 mHz (23 sec period) in preflare polarization variations; no such component was found for preflare temperature. Recommendations for future areas of investigation using high-resolution solar radio instrumentation are suggested.

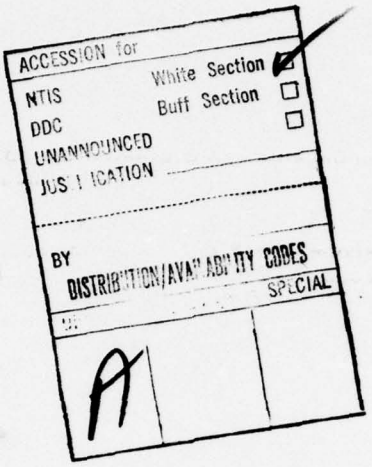

Preface

The author wishes to acknowledge the support provided to this program by Dr. Jules Aarons, Chief of the Trans-Ionospheric Branch, and to Mr. John P. Castelli, Chief of the Solar Radio Section.

Special acknowledgements go to Dr. Paul M. Kalaghan, initiator of the In-House Work Unit 46430302, whose insight and laborious computer efforts provided the material used in Section 2 and to Mr. Neal Grossbard, mathematician, for the techniques of power spectrum analysis and the extensive programming of the AFGL CDC-6600 computer to obtain the plots used in Section 4.

I wish to thank my colleagues (at AFGL) Drs. Donald A. Guidice and David Richards, (Boston University) Prof. Michael D. Papagiannis and Dr. Fred Wefer, (NELC Laposta Observatory) Dr. Max Blieweiss, and the excellent staff at the NEROC Haystack Observatory, for their many discussions and encouragements to this study. Research at the Haystack Observatory of the Northeast Radio Observatory Corporation (NEROC) is supported by the National Science Foundation under Grant MPS71-02109A07.

Finally, the author is indebted to his two daughters, Erika and Sonya Straka, for their assistance in preparing this report.

Contents

Illustrations

Tables

High Resolution Solar Radio Activity Investigations

1. INTRODUCTION

The ability to monitor individual solar active regions with high spatial resolution at microwave wavelengths by the use of large radio-telescopes, provides an opportunity of detecting changes in the region that could be a prelude to eruptive solar activity. Monitoring the slowly varying component (SVC) of emission from the region, which varies as the magnetic field strength, temperature, and density change in the region, appears to provide a sensitive indicator of possible activity in the region. Numerous studies of active region emission characteristics have been made.[1] A few of these studies have related to the potential of using increased radio brightness temperatures (T_b) as a possible tool for flare forecasting. Kundu[2] found that, at a 3-cm wavelength, regions with high brightness temperatures and small size had a high probability of occurrence for flare and radio burst activity. At 3-mm wavelength, using the 15-ft diameter Aerospace Corporation antenna, Simon[3] observed one case where an increased T_b was observed prior to a Class 1 flare. Later, Mayfield, Higman, and Samson[4] showed that optical flares of Class 2

(Received for publication 7 November 1977)

1. Kundu, M.K. (1965) Solar Radio Astronomy, Interscience Publishers, New York, p 168.
2. Kundu, M.K. (1959) Ann. Astrophys. 22:1.
3. Simon, Michael (1965) Astrophys. J. 141:1513.
4. Mayfield, E.B., Higman, J.A., and Samsor, C.F. (1970) Solar Phys. 13:372.

or greater could be expected to occur within the 24 hr after the 3.3-mm region T_b increased more than 8.8% and had a temperature gradient of 0.5%/heliographic-deg or greater. The gradient was measured from the 2% isotherm to the highest temperature point. A problem with the gradient determination, however, is the smoothing caused by the large half-power-beamwidth (HPBW) of the antenna, which for the Aerospace antenna was 2.8 arc-min. Blieweiss et al,[5] indicated that in effect the 8.5% and 0.5%/deg of the Aerospace measurements translate to 8.5% and (0.5%/deg) × (HPBW) = 5%; or in other words, that the measurements were really using only an enhancement threshold, and that the threshold value was 5%.

A technique for forecasting solar flares of classes 1N or 1B was developed by White[6] from extensive Aerospace 3-mm observations. He found that: (1) all positive flare-history plage regions with peak enhancements ≥ 8.4% will produce class 1N flares; (2) all positive flare-history plage regions with peak enhancements ≥ 9.7% will produce class 1B flares; and (3) at best, the probability of a class 1N flare in a virgin region never exceeds 10 to 20%.

At 8.6-mm wavelength, Withbroe and Vernazza[7] examined active-region flare rates and found that the probability for large solar flares increases significantly for high 8.6-mm brightness temperatures.

In addition to predicting flares from the region brightness temperatures, research by the Japanese has shown[8,9] that flux ratios (at centimeter wavelengths) of the active-region slowly varying component can be used as a predictor that the region will be a proton flare producer. This spectral approach to the active region emission appeared to be a most promising short- to medium-term predictor of solar proton activity, and is examined in greater detail in this report.

Another promising technique for the forecasting of flare activity comes from emission variations that precede the flare, such as: (1) periodic fluctuations in the brightness temperatures,[10] and (2) changes in the centimeter wavelength emission polarization one-half to a few hours before the flare.[11,12]

AFGL, through In-House Work Unit 46430302, High Resolution Solar Activity Investigation, has conducted studies and supported contractual studies to determine the radio characteristics of the active-region slowly varying component that may be potential indicators of eruptive flare and proton-flare activity. This report describes three specific in-house efforts: (1) the use of 9.1 cm, 8 mm and 3 mm active-region spectral data as a short-term proton event predictor (Section 2), (2) observations of a proton-flare event with dual circular polarization at 3.8 cm wavelength (Section 3), and (3) the power spectrum analysis of preflare variations in brightness temperature and polarization from active regions at 3.8-cm wavelength (Section 4). Conclusions drawn from the high-resolution studies are then presented in Section 5.

(Because of the large number of references cited above, they will not be listed here. See Reference Page 43, for References 5 through 12.)

2. ACTIVE REGION SPECTRAL DATA AS PROTON EVENT PREDICTORS

2.1 Introduction

Through the use of large radiotelescopes it has been possible to monitor the slowly varying component (SVC) of radio emission from localized activity centers on the sun. Different radio wavelengths probe different altitudes of the solar atmosphere above the activity center; with the short-wavelength millimeter emission coming from the photosphere and the centimeter-wavelength emission from the transition zone up into the lower corona at the longer wavelengths. A comparison of emission at the different wavelengths provides information on changes in electron temperature, electron density, and magnetic field intensities that occur in different solar altitudes prior to flare eruptions. Insight into the physical conditions that exist for proton producing regions should be available from these types of measurements. Early work by Tanaka and Kakinuma,[8] where they examined 62 regions during 1959 to 1961, showed that when the 3.2-cm to 7.5-cm wavelength flux density ratio exceeded the value of one, the region produced a proton flare. It was suggested that if the magnetic field intensities increased as the region developed, the 3-cm wavelength gyroresonance levels of the 2nd and 3rd harmonics would rise from the cool chromosphere where they normally are found into the hotter corona, whereas the 7.5-cm emission levels would change little, thus increasing the ratio. Increased magnetic fields could then serve as good proton accelerators at the time of the flare. Nakajima[9] found that the 3-cm to 1.8-cm flux density ratio also increased for a proton producing active region. The SVC at 1.8-cm decreased prior to the flare and the 3 cm tended to increase. It was felt that increased plasma heating in the region prior to the proton flare caused the optically-thin source at 1.8 cm to have reduced flux density and the optically-thick 3 cm source to increase in flux density. This result, however, was based on the multiple proton flaring of one active region (McMath 11976) in July-August of 1972.

To expand on these investigations of spectral characteristics of the SVC from the active regions as possible long-term predictors of proton activity, a statistical study using extensive active-region data at three wavelengths was performed at AFGL. The data base is from the 1968 to 1970 spectroheliograms provided by Stanford University (9.1 cm), Air Force Cambridge Research Laboratories* (8.6 mm), and the Aerospace Corporation (3.2 mm).

2.2 Observational Data

There were a total of 169 days during the 1968 to 1970 period where all three observatories were able to obtain high-spatial-resolution measurements on the

*Now Air Force Geophysics Laboratory (AFGL).

same activity centers. The number of days when common observations could be obtained was considerably reduced by equipment problems, inclement weather, and scheduling conflicts at each of the observatories. All the telescopes had spatial resolutions of about 3 to 4 arc-min. Narrow beams were obtained from single solid-surface parabolic radiotelescopes at Aerospace and AFCRL, and by a pencil-beam interferometer array at Stanford.

2.3 Data Processing

The approach used in this investigation was to generate a program for the CDC 6600 computer which would take the various radio heliograms, which were given as arrays of antenna temperature values, and systematically locate the enhanced active centers relative to a background or quiet level. Once these features were found, their positions were determined by locating the maximum of several Gaussian fits thru neighboring grid points (see Figure 1). These positions were then translated into the corresponding heliographic coordinates which were compared with optical maps of the Sun in the NOAA Solar-Geophysical Data to identify the associated McMath plage region. Only those regions for which the position at each wavelength was within one-half a beamwidth of the position obtained at the other two wavelengths, were retained and processed. This position deviation criterion used to define a region with near coincidence of its maximum intensities to other regions caused numerous regions to be rejected for analysis.

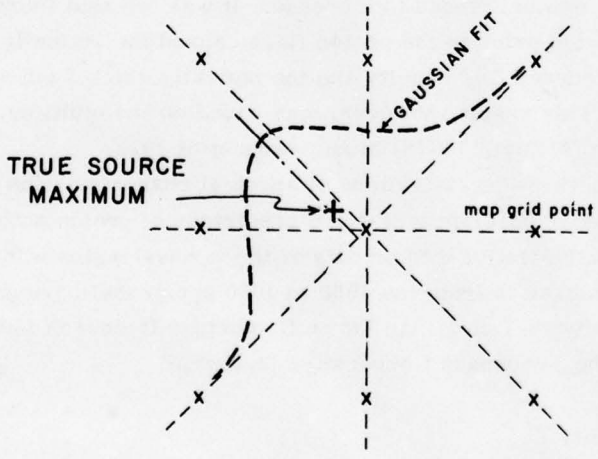

Figure 1. Gaussian Best Fit Curves Through the Measured Maximum Signal Map Grid Point in Order to Determine the True Source Maximum Level and Position

The apparent size of each radio emission region was next determined. Temperature contour levels of the features were obtained and the half-power intensity levels of the Gaussian curves in eight radial directions (shown in Figure 1) were used to establish the widths of the sources. Comparions of the source widths in the different directions allowed the determination of sizes for overlapping features.

Apparent flux density values were obtained from the apparent source size and the measured brightness temperatures.

Corrected source sizes were determined by taking into account the Gaussian-beam effects on the assumed Gaussian-source distribution. True source flux values were then computed using the corrected source sizes.

From the source sizes, apparent flux densities and true flux densities, various combinations of these region characteristics were formed and statistically compared with the region's proton-producing activity. Table 1 lists the 22 different prediction parameters formed for which statistical analyses were performed. Parameters (14), (15), (19), and (20) are computed spectral indices for the 9.1-cm/8.6-mm and the 8.6-mm/3-mm apparent and true flux densities. The spectral index (SI) is determined by the ratio of the log of the wavelength ratio to the log of the inverse of the flux density ratio; that is, $SI = \log(\lambda_1/\lambda_2)/\log(F_2/F_1)$.

Histogram plots of each of these 22 parameters for the 169 days of observations (681 region cases) were drawn. Those region cases having associated satellite measured proton events were marked as open circles, and those having ionospheric level 30 MHz polar cap absorption events (PCA's) were marked as solid circles (see later in Figures 2 to 4). Associations with the proton events were allowed up to one day prior to the flare event. Some regions were measured several times during one observation day. No attempt was made to obtain an average value for these multiple measurements, instead each case was treated individually. This allows for possible short term changes that could have occurred prior to the proton flare.

The "Catalog of Solar Particle Events 1955-1969" by Svestka and Simon[13] was the primary source for proton event data. Additional updated data were generously provided by Smart and Shea[14] from their event catalog. Table 2 lists the proton events used in the analysis. Also given are the associated McMath plage region in which the parent flare occurred, the sensor that detected the event, the energy range of the detector, the proton count and 30 MHz decibel absorption value, and the dates on which the preflare active-region measurements were made. A total of twenty-five proton events occurred when mapping data was available from all three observatories.

---

13. Svestka, Z., and Simon, P. (1975) Catalog of Solar Particle Events 1955-1969 D. Reidel Publ. Co., Dordrecht Holland/Boston USA.

14. Smart, D., and Shea, P. (1976) Private Communications.

2.4 Results

The statistical properties of the various prediction parameters computed in the analysis are listed in Table 1. Mean values for all 681 region measurements, standard deviations for all the regions, mean values for those regions associated with proton events, and the standard deviations for the proton producing regions are given in Table 3.

Table 1. Prediction Parameters

Parameter	Units	Description
(1) LAT	°Lat	Latitude of source + 50°
(2) LONG	°Long	Carrington Longitude of source
(3) ROS	arc min	Radius of Separation (mean for three λ sources)
(4) S9.1	arc min	Size of 9.1 cm source
(5) S8	arc min	Size of 8 mm source
(6) S3	arc min	Size of 3 mm source
(7) RPAR	*s.f.u./arc min	FAS/ROS (FA = apparent flux)
(8) RPRR	s.f.u./arc min	Σ(FA9.1 + FA8) / ROS
(9) TPAR	s.f.u./arc min	FTS/ROS (FT = true flux)
(10) TPRR	s.f.u./arc min	Σ(FT9.1 + FT8 / ROS
(11) FA9.1	s.f.u.	Apparent 9.1 cm flux
(12) FA8	s.f.u.	Apparent 8 mm flux
(13) FA3	s.f.u.	Apparent 3 mm flux
(14) QAL	-	Spectral Index 9.1 cm to 8 mm (FA)
(15) QAH	-	Spectral Index 8 mm to 3 mm (FA)
(16) FAS	s.f.u.	Σ(FA9.1 + FA8 + FA3)
(17) FT9.1	s.f.u.	True 9.1 cm flux
(18) FT8	s.f.u.	True 8 mm flux
(19) FT3	s.f.u.	True 3 mm flux
(20) QTL	-	Spectral Index 9.1 cm to 8 mm (FT)
(21) QTH	-	Spectral Index 8 mm to 3 mm (FT)
(22) FTS	s.f.u.	Σ(FT9.1 + FT8 + FT3)

*Solar Flux Unit (s.f.u.)

Table 2. Proton Event Table

Date of Proton Flare	Event No.	McMath Region	Satellite Sensor	Proton Count* or dB Absorption	Proton Energy (MeV)	Preflare Observation Dates
07 Jun 68	1	9428/9423	IMP4	0.08	> 9	7 Jun 68
21 Jul 68	2	9530	IMP4	5.7	> 0.8	21 Jul 68
06 Aug 68	3	9567	IMP4	0.2	> 9	5, 6 Aug 68
19 Aug 68	4	9593	IMP4	0.2	> 9	19 Aug 68
04 Sept 68	5	9630	PION8	0.18	>14	4 Sept 68
26 Sept 68	6	9687	IMP4	13.0	> 9	25 Sept 68
			RIOM	*0.8		
01 Nov 68	7	9740	IMP4	151.67	>10	1 Nov 68
			RIOM	*5.9		
21 Nov 68	8	9772	IMP4	18.5	>10	21 Nov 68
17 Jan 69	9	9873	IMP4	1.7	> 9	16 Jan 69
08 Mar 69	10	9966	IMP4	0.15	> 9	8 Mar 69
12 Mar 69	11	9966	IMP4	2.18	>10	11 Mar 69
			RIOM	*0.7		
24 Mar 69	12	9994	IMP4	41.0	> 0.8	24 Mar 69
29 Apr 69	13	10055	IMP4	0.3	> 9	28, 29 Apr 69
05 Jun 69	14	10134	PION8	0.18	>14	5 Jun 69
07 Jun 69	15	10134	PION8	0.18	>14	6, 7 Jun 69
			RIOM	*1.4		
11 Jun 69	16	10134	PION8	0.38	>14	10, 11 Jun 69
17 Sept 69	17	10317/10309	IMP5	1.5	> 1	16 Sept 69
25 Sept 69	18	10326	IMP5	14.92	>10	24, 25 Sept 69
			RIOM	*0.7		
30 Sept 69	19	10344	IMP5	89.0	> 1	29, 30 Sept 69
18 Nov 69	20	10432	IMP5	0.15	>10	17, 18 Nov 69
20 Nov 69	21	10432	IMP5	9.0	> 1	19, 20 Nov 69
23 Nov 69	22	10432	PION9	1.2	>14	22, 23 Nov 69
13 Dec 69	23	10477	IMP5	2.9	> 1	13 Dec 69
23 Dec 69	24	10499/10477	IMP5	14.0	> 1	23 Dec 69
07 Mar 69	25	10618	IMP5	93.4	>10	7 Mar 70
			RIOM	*5.1		

*Proton Count = protons$(cm^2 sec\ ster)^{-1}$

Table 3. Statistical Properties of the Various Prediction Parameters

Prediction Parameters	Mean (All regions)	Stand. Dev. (All regions)	Mean (Proton event associated)	Stand. Dev. (Proton event associated)
(1) LAT	79.9	15.	54.9	17.0
(2) LONG	155.9	105.5	119.2	66.4
(3) ROS	1.49	0.57	1.16	0.65
(4) S9.1	1.79	0.72	2.50	0.86
(5) S8	2.74	1.15	2.30	1.07
(6) S3	2.60	0.83	2.26	1.14
(7) RPAR	19.	19.3	40.6	36.4
(8) RPRR	12.9	21.9	27.4	25.3
(9) TPAR	53.0	48.9	102.7	89.7
(10) TPRR	26.67	43.4	57.5	62.4
(11) FA9.1	5.77	5.65	10.9	8.4
(12) FA8	5.27	7.08	10.6	14.4
(13) FA3	11.3	4.7	14.8	6.0
(14) QAL	1.03	0.26	0.93	0.38
(15) QAH	1.9	0.43	1.58	0.68
(16) FAS	22.3	14.6	36.3	24.2
(17) FT9.1	10.5	10.9	21.2	19.1
(18) FT8	12.8	15.3	19.9	19.2
(19) FT3	41.5	26.2	49.3	29.9
(20) QTL	1.14	0.37	0.94	0.40
(21) QTH	2.27	0.66	1.94	0.74
(22) FTS	64.8	41.2	90.5	55.7

The parameters where the sum of the region flux densities is divided by the mean radius of separation all tend to show significant increases in their mean values for the proton regions. This indicates that the more intense sources that have their centers of emission (at the different wavelengths) closest together are most likely to produce a proton flare event. Figure 2a shows the histogram plot of one of these parameters, $\Sigma F^T/ROS$. This plot shows that, although the mean for the proton regions is higher than the non-proton regions, there is a large spread of values for the proton/PCA regions. One cannot, therefore readily assign any threshold value for prediction purposes. An examination of the plot of ROS, Figure 2b, does reveal a slight shift towards the smaller radius of separation for the proton sources. And, from Figure 3a, one observes the tendency of proton events to have larger sums of the three wavelength True Flux values, ΣF^T.

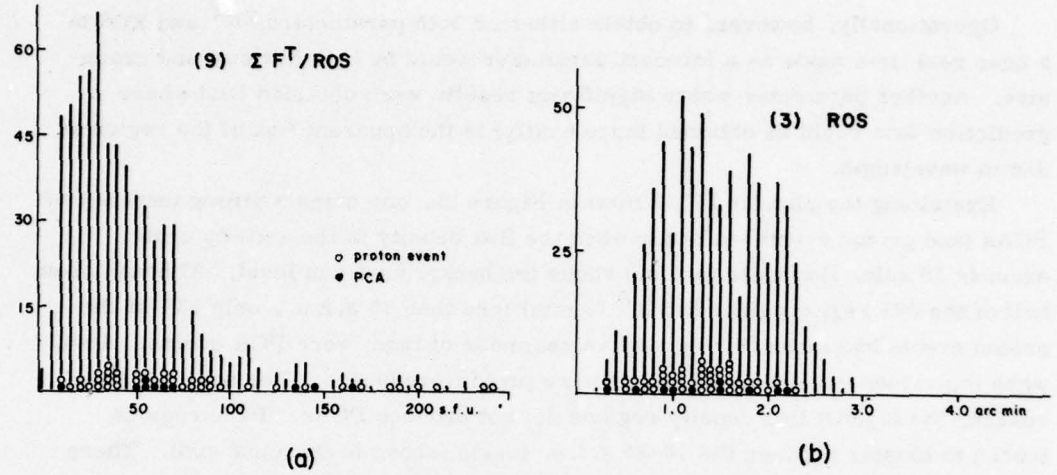

Figure 2. Parameter Histograms. (a) Histogram of parameter (9). Sum of the true fluxes at 9.1 cm, 8 mm, and 3 mm divided by the mean separation of the sources at the three wavelengths for all the measured active regions, with the proton event distributions, (b) same histogram, but for parameter (3) the mean radius of separation for the sources at the three wavelengths

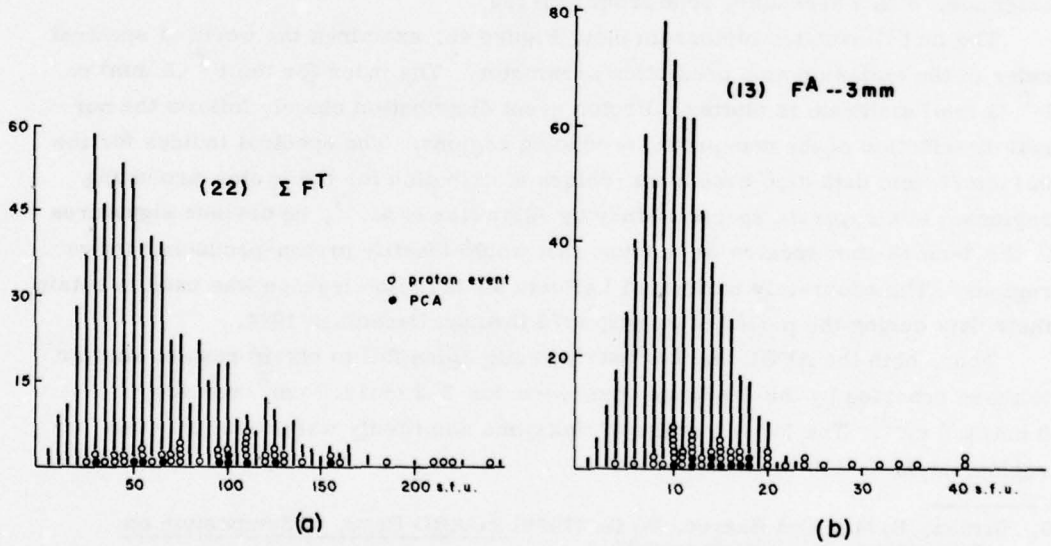

Figure 3. Parameter Histograms. (a) Same histogram, but for parameter (22) the sum of true fluxes for the three wavelengths, (b) same histogram, but for parameter (13) the apparent flux at 3 mm

Operationally, however, to obtain either or both parameters ΣF^T and ROS in a near real time mode as a forecast parameter would be both difficult and expensive. Another parameter where significant results were obtained (and where prediction data could be obtained more easily) is the apparent flux of the region at 3-mm wavelength.

Examining the plot for F^A (3 mm) in Figure 3b, one notes a strong tendency of PCAs (and proton events) to occur when the flux density in the activity center exceeds 10 solar flux units (s.f.u.) above the background-sun level. Although about half of the 681 region values had F^A (3 mm) less than 10 s.f.u., only 13% of the proton events had these flux density values; none of them were PCA events. Also, when the values exceed 25 s.f.u. all were proton-producers. For some unknown reason, the highest flux density regions did not produce PCAs. PCA-regions tended to cluster between the 10-20 s.f.u. levels (above background sun). These significant forecasting results at 3-mm wavelength for proton events very nicely parallel the Aerospace results for flare forecasting.[4,6]

Two other parameter plots merit comment. Figure 4a shows a clustering of the proton producing regions around 60-90° Carrington longitude. This is at variance with what Straka and Barron[15] found for PCA flare producing centers for 1966 to 1968 solar data, and what Dodson and Hedeman[16] had for 1962 to 1966 data. In both studies, a primary zone of concentration was from 160-230° Carrington longitude, with a secondary zone from 320-350°.

The last illustrated histogram plot, Figure 4b, examines the worth of spectral index of the emission as a prediction parameter. The index for the F^T (8 mm) to F^T (3 mm) emission is plotted. Proton event distribution closely follows the normal distribution of the non-proton producing regions. The spectral indices for the 9.1-cm/8-mm data also have a non-unique distribution for the proton-producing regions. In a separate spectral study by Bleiweiss et al [17], no obvious signatures in the 2-cm/8-mm spectra were found that would identify proton-producing active regions. The accurately calibrated LaPosta 60-ft radiotelescope was used to obtain their data during the period of August 1972 through December 1974.

Thus, both the AFGL and LaPosta investigations fail to obtain results similar to those reported by the Japanese observers for 3.2 cm/7.5 cm[8] and for 3 cm/1.8 cm[9]. The latter results of Nakajima admittedly were from only one region, McMath 11976.

---

15. Straka, R.M., and Barron, W.R. (1970) AGARD Proc. of Symposium on Ionospheric Forecasting 49:10-1.

16. Dodson, W.H., and Hedemen, E.R. (1967) Structure and Development of Solar Active Regions, I.A.U. Symposium No. 35, ed. K.O. Kiepenheuer, D. Reidel Publ. Co., Dordrecht, Holland.

17. Bleiweiss, M.P., Wefer, F.L., and Hurst, M.D. (1976) NELC Tech Rpt. TR-1999.

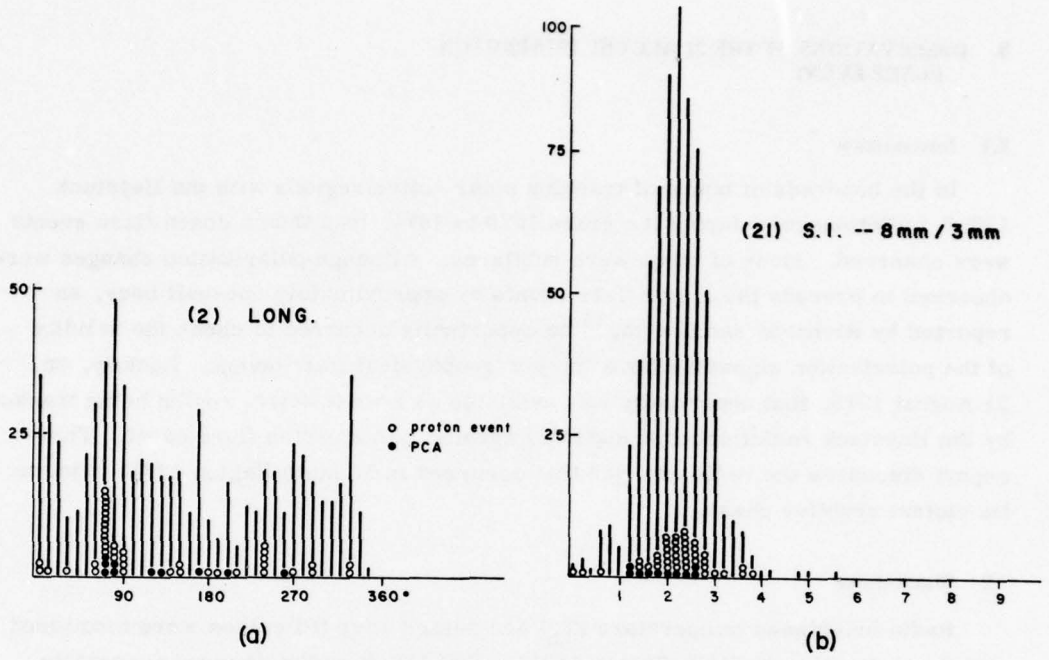

Figure 4. Parameter Histograms. (a) Same histogram, but for parameter (2) the Carrington longitude of the active region. (b) Same histogram, but for parameter (21) the spectral index for the 8 mm to 3 mm flux

To summarize the results of the AFGL (AFCRL) study on the spectral characteristics of active regions at 9.1 cm, 8 mm, and 3 mm, as they apply to proton producing regions, the following can be said:

(1) The best indicator of a proton-producing active region was the increase of 3-mm wavelength apparent flux density; in particular, if the region had an excess flux density greater than 10 s.f.u. above the background-sun level;

(2) The probability for the region to produce a proton flare increases if the active-region emission at 9.1 cm, 8 mm, and 3 mm becomes high and the radius of separation for the centers of emission at the different wavelengths decreases—that is, clustering occurs,

(3) No indication has been found for the 9.1-cm/8-mm or the 8-mm/3-mm spectral indices that shows that they can be used to forecast proton and/or PCA events from activity centers on the sun.

3. OBSERVATIONS OF THE 21 AUGUST 1975 PROTON FLARE EVENT

3.1 Introduction

In the hundreds of hours of tracking solar active regions with the Haystack 120-ft radiotelescope during the years 1970 to 1974, less than a dozen flare events were observed. Many of these were subflares. Although polarization changes were observed to precede the minor flare events by approximately one-half hour, as reported by Richards and Straka,[11] no opportunity occurred to check the validity of the polarization signature for a 'major' geophysical flare-event. Luckily, on 21 August 1975, that opportunity was available as a weak active region being tracked by the Haystack radiotelescope suddenly erupted into a proton flare event. This report discusses the radio changes that occurred in McMath Region 13811 prior to its violent eruptive phase.

3.2 Observations

Radio brightness temperature (T_b) and polarization (P) values were monitored at 3.7-cm wavelength from Region 13811. The 120-ft radiotelescope accurately tracked the region and obtained data samples once every 3 sec of time. Right and left circular polarizations were monitored simultaneously.

Because of the large half-power beamwidth of the antenna (4.4 arc min), the measured brightness temperature T_b is a diluted value of the source brightness temperature T_s by the ratio of the solid angle of the source divided by the solid angle of the antenna beam. Thus, for a 1-arc-min source, the measured brightness temperature would be reduced by $(1)^2 / (4.4)^2$, or approximately one-twentieth. However, if the source brightness temperature (T_s) is much greater than that of the background region, the measured (antenna) temperature increase may be quite visible. For example, if T_s is 20 times the background temperature, the measured temperature increase, even with a one-twentieth dilution due to the solid angle ratio, would be of the order of the background temperature.

To examine the dilution effect on polarization, assume the source has a large unpolarized halo with a small diameter polarized core, similar to that found at 3-cm wavelength by Kundu.[2] Let the unpolarized halo have an angular diameter equivalent to the antenna HPBW (4.4 arc min) and have a brightness temperature for the halo, T_h, of 1×10^5 °K. The brightness temperature of the polarized core, T_c, will parametrically be selected at 1×10^6, 2×10^6, 1×10^7 and 1×10^8 °K. The measured polarization fraction is given by the equation

$$P = \frac{T_c \Omega_c}{T_c \Omega_c + T_h(\Omega_h - \Omega_c)}$$

$$= \frac{1}{1 + \frac{T_h}{T_c}\left(\frac{\Omega_h}{\Omega_c} - 1\right)}$$

where Ω_c is the core solid angle and Ω_h is the solid angle of the halo (which is set equal to the solid angle of the antenna, Ω_a).

The polarized core will be assumed to be 100% circularly polarized, and vary in size from 0.2 to 4.4 arc min. Results of this analysis are plotted in Figure 5. For a 1.0-arc min core size, the measured polarization for a 2×10^6 °K core would be 52%, or a dilution of 48%. However, this measured polarization percentage increases to 73%, 84%, and 98% as the source temperature of the core increases to 5×10^6, 1×10^7, or 1×10^8 °K, respectively. Thus, the dilution can be small if the core temperature is very high. Lang[12] has shown the 3.7-cm emission just prior to the flare comes from a small-sized region, size ≤7 arc sec, with temperature $T_b \geq 10^6$ °K and circular polarization of 90 ± 10%; during the flare $T_b \geq 3 \times 10^6$ °K. This would mean about a 5 to 10% polarization change on the recorded data which is easily detectable with the Haystack system (it can detect a 0.5% polarization change).

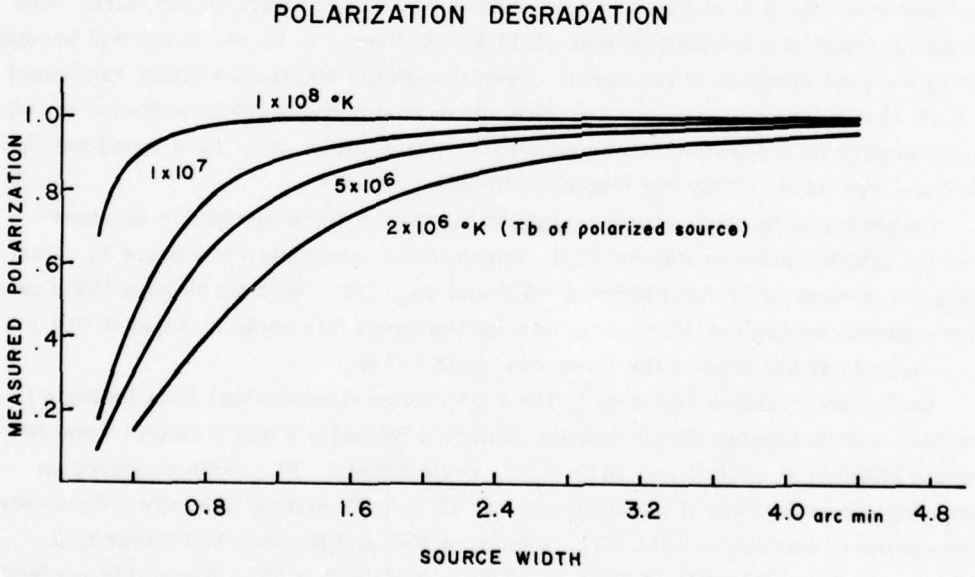

Figure 5. Polarization Degradation for a 100% Polarization Core Source of Varying Source Width Surrounded by an Unpolarized Halo Source the Size of the Beam HPBW (4.4 arc min) as a Function of Various Brightness Temperatures for the Polarized Core

On the 21st of August 1975, the first hour of observations were devoted to making detailed maps of McMath Region 13811 in order to maximize the pointing-tracking on the region. After several scans through the region, it became apparent that unusual activity was occurring in the region. Region tracking was immediately begun at 1430 UT. The recorded brightness temperature, however, continued to drop over the next 30 to 40 min from a level of about 31,000 °K to a level of 28,000 °K. This was just above the background sun level of 22,000 °K.

These temperatures were low for a region that had numerous subflares and radio-burst activity earlier in the day. For example, Types III and II metric wavelength bursts were recorded from a subflare at 0514 UT, ten hours prior to the proton flare. This subflare had a radio 'min-U-burst' with the following solar flux densities (1 s.f.u. = 1×10^{-22} W/m^2/Hz): 17.9 at 8800 MHz, 12.2 at 4995 MHz, 10.4 at 2695 MHz, 4.5 at 1415 MHz, and 7.9 at 606 MHz. Castelli, Aarons, and Michael[18] have shown that when the 8800 MHz flux exceeds 1000 s.f.u. and the burst has a U-shape with high flux densities at metric decimetric wavelengths, a major proton event can be expected to occur from the flare.

Because of the low 3.7-cm wavelength brightness temperature from Region 811 (McMath 13811), no major flare activity was anticipated to happen. But at about 1514 UT, the signal gradually increased at first and then rapidly increased until the equipment saturated at 1519 UT (see Figure 6b). Polarization changes are shown in Figure 6a. The flare, importance 1N, was a proton producer. During the observations no obvious changes in polarization occurred to warn of the flare. The small reversal of polarization near 15:11:50 UT from + 0.1% to -0.2% was brought out in the post analysis of the burst. Even though the Haystack system can detect a 0.1% change in polarization, it is difficult to assign too much importance to this small change as a possible flare predictor. The earliest start time found for the Hα flare was 1509 UT (by the Wendelstein Observatory).

Hα photographs taken prior-to and during the 1N flare by the Air Weather Service SOON station at Ramey AFB, Puerto Rico, are shown in Figure 7. Maximum Hα intensity occurred between 1517 and 1519 UT. McMath Region 13811 is a high-latitude region (26°N) associated with the new cycle spots of Sunspot Cycle 21. Its longitude at the time of the flare was about 7 °W.

Radio observations reported in the NOAA Solar-Geophysical Data indicate that Durnten and Weissenan Observatories reported Intensity 3 and 2 metric Type IV bursts starting at 1518.7 and 1518.8 UT, respectively. Ft. Davis reported an Intensity 3 metric Type II burst starting at 1519.3 UT and an Intensity 3 dekametric Type II burst starting at 1528 UT. Sagamore Hill and Boulder had Intensity 3 dekametric Type II bursts at 1521.8, 1522.5, and 1524.6 UT. Favorable conditions

18. Castelli, J.P., Aarons, J., and Michael, G.A. (1967) J. Geophys. Res. 72:5491.

for a proton event, that is, the classic Type II-IV bursts, were thus indicated by the sweep-frequency spectral data.

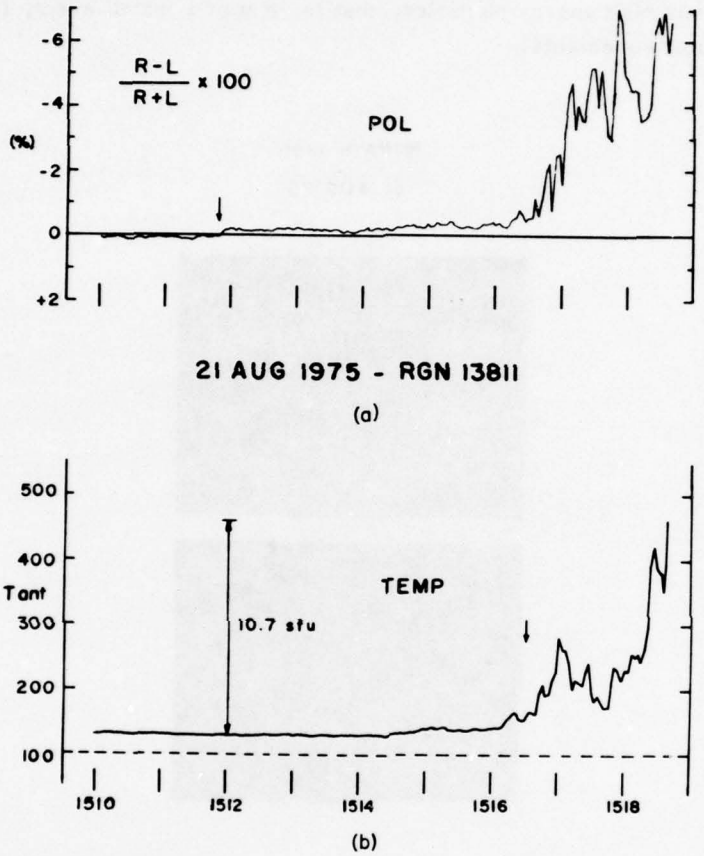

Figure 6. Measured Polarization and Temperature Changes. (a) Measured 3.8 cm polarization prior to the proton flare of 21 August 1975. (b) Measured 3.8 cm antenna temperature prior to the proton flare of 21 August 1975. The 100 level represents background quiet sun level.

The centimeter-wavelength data recorded at Sagamore Hill showed the classic U-shaped spectrum, with a peak flux at 8800 MHz of 1135 s.f.u. (see Figure 8). The radio criteria for signifying a proton-flare event were amply met. The integrated flux density of the burst at 8800 MHz gave an estimate of 0.5 dB absorption for the expected PCA (it was measured to be 0.6 dB). The ω_3/ω_2 computation of

Bakshi and Barron[15] (that is, the ratio of the cm-λ maximum-emission frequency to the dm-λ minimum-emission frequency) gave an estimated slope for the > 10 MeV to > 60 MeV proton-energy spectrum of about 1.1. This indicated that the proton event had many high energy particles, that is, it was a 'hard' event, (later confirmed by satellite measurements).

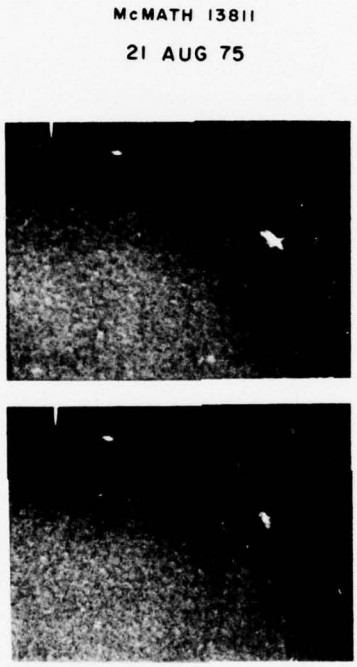

Figure 7. Hα Photographs of Proton Flare in McMath 13811 on 21 August 1975 Supplied by USAF, Ramey AFB, Puerto Rico. (a) 1N proton flare at 1521 Z (flare max about 1518 Z). (b) Preflare photo at 1358 Z (flare start at 1509 Z

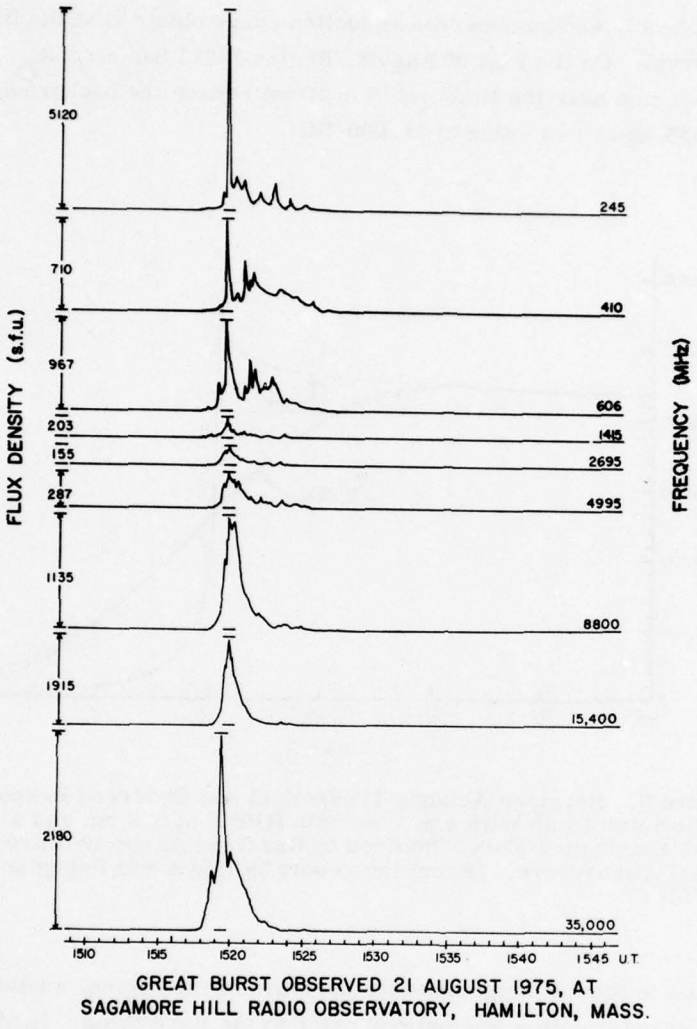

Figure 8. Great Burst Observed 21 August 1975, at Sagamore Hill Radio Observatory, Hamilton, MA

3.3 Discussion

One reason for the region's low brightness temperature may be the result of its near-the-limb position. The reduction in signal that takes place near the limb for the Haystack 4.4-arc min beam is shown in a figure from the report by Kogut and Papagiannis,[19] Figure 9. This figure shows the theoretical curve of the reduction of the limb brightened T_b curve (derived from ray-tracing the Harvard

19. Papagiannis, M. D., and Kogut, J. A. (1975) AFCRL Tech. Rept. TR-75-0430.

Model Atmosphere), and an observed reduction curve obtained at the limb during a quiet-sun interval. On the 21st of August, Region 13811 had an $r/R_{\odot}$ of about 0.95. This position near the limb would in effect reduce the background undisturbed-sun level by 23% down to a value of 17,000 °K.

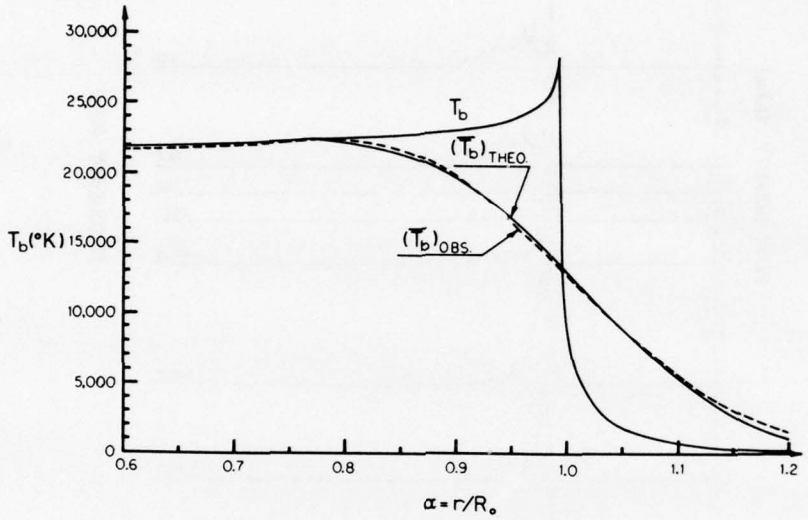

Figure 9. Haystack Antenna Theoretical and Observed Response at the Solar Limb With a 4.4 arc min HPBW at 3.8 cm and a Limb Brightened Model Obtained by Ray Tracing the Harvard Model Atmosphere. [From the report by Kogut and Papagiannis (1975)]

In addition to the low brightness temperature of the region, another surprise was the lack of polarization fluctuations prior to the flare event. In about 12 flare events observed with the Haystack antenna during 1970 to 1975, all had polarization variations prior to the flares. Section 4 of this report describes eight such events. Observing at the N.R.A.O. facility at 3.7 and 11 cm wavelengths, Lang[20] reported seeing strong polarization changes 1 hr prior to a flare in a region. When tracking this same region for three days in advance (40 hours of observations), however, he observed no substantial changes in polarization were detected.

The activity from Region 13811 was also peculiar in that it was a new region just having appeared one day before the proton flare occurred. In its less than three days presence on the disk (before it disappeared at the west limb), a total of

20. Lang, K.R. (1977) Solar Phys. 52:63.

26 flares were recorded in the region. Many of these flares produced sudden ionospheric disturbances (SID's), as was previously mentioned. Nine of these SID's were recorded on 22 August, the last day the region was visible on the disk.

3.4 Conclusion

The observations of active region McMath 13811 up until the time of its producing a proton flare brought out several important forecasting results. First, it showed that the observed brightness temperature of a region could at 3-cm wavelength, actually decrease prior to its flaring. Second, it is possible that no significant polarization changes or variations may occur in advance of the flare (in the case observed, a proton flare). Third, near-the-limb observations of active regions may limit the forecasting information obtainable from high-resolution solar radio monitoring.

The unusual and unexpected activity from McMath 13811, young in existence, strongly illustrates the conclusion that in some instances the best prediction one can make about a region's activity is that it can be expected to be unpredictable.

4. POWER SPECTRUM ANALYSIS OF PREFLARE VARIATIONS AT 3.8 CM WAVELENGTH

4.1 Introduction

Optical astronomers have reported numerous observations of periodicities being detected in the solar atmosphere, notably the 5-min vertical-velocity oscillations detected by periodic Doppler shifts of photospheric and lower-chromospheric lines. (See Noyes[21] for a review article.) These fluctuations are measured from the quiet background sun. Using a very high spatial resolution radiotelescope at 3-mm wavelength, Simon and Shimabukuro[22] also detected a strong oscillation component with a period of 180 sec in the background sun. Lang[23] reported observing quasi-periodic changes at 3.7-cm and 11-cm wavelengths coming from the chromosphere-corona transition region, using the Owens Valley Radio Observatory and National Radio Astronomy Observatory interferometer systems. He found a band of periods from 200 to 400 seconds for the quiet sun.

The possibility of detecting oscillations in the solar active regions is of great interest to radio astronomers and those seeking signatures of potential flare activity. Russian observers[24, 25], for example, using the large Pulkovo radiotelescope at

21. Noyes, R.W. (1967) Proc. I.A.U. Symp. No. 28, 293.
22. Simon, M., and Shimabukuro, F.I. (1971) Astrophys. J. 168:525.
23. Lang, K.L. (1974) Astrophys. J. 192:777.
24. Yudin, O.I. (1968) Soviet Phys. Doklady 13:503.
25. Dursova, M.S., Dobrin, M.M., and Yudin, O.I. (1971) Nature 229:72.

3.3-cm wavelength detected quasi-periodic fluctuations of brightness temperature with periods of about 250 and 700 seconds. Later, Gelfreykh et al[10] reported that at 4 cm the periodicities appeared more clearly on days of higher solar activity.

Changes in polarization as well as brightness temperature were observed by Richards and Straka[11] to occur in the active region about 1/2-hr prior to flare activity. These observations were made with the NEROC 120-ft Haystack radiotelescope at 3.8-cm wavelength. A review of the 1970-1971 Haystack records was made to find possible periodicities in the polarization of the radiation from active regions. Figure 10 shows one result from this investigation that was presented by Straka et al[26] at the Spring 1972 Solar physics Division meeting of the AAS at

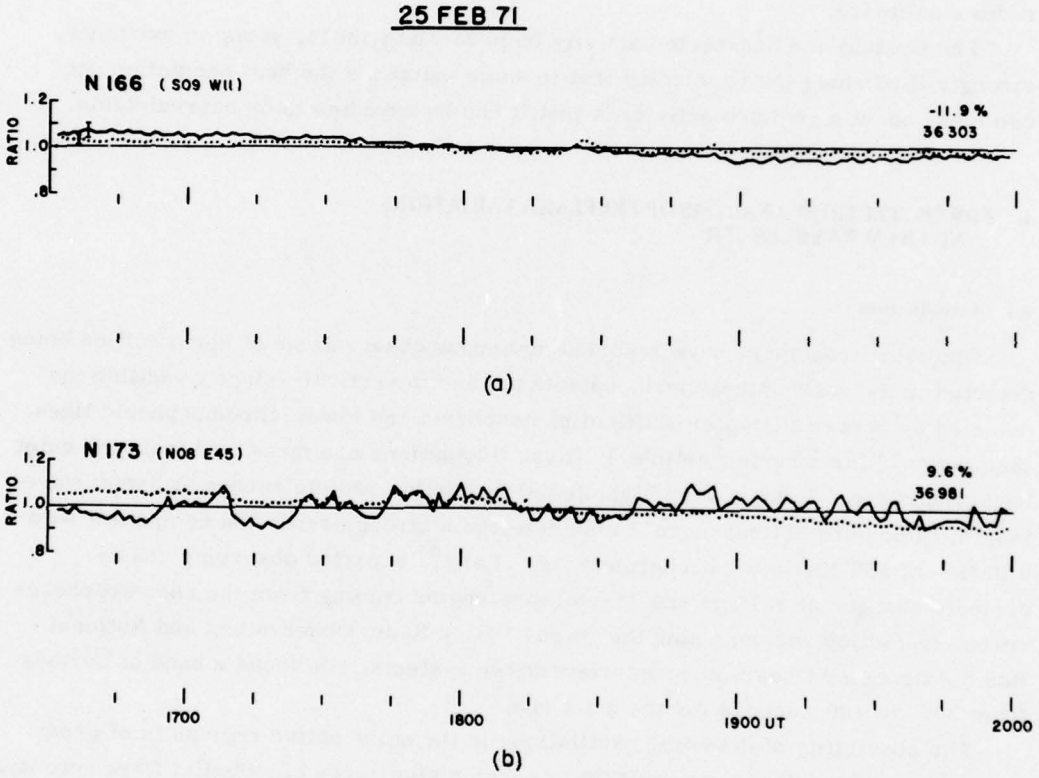

Figure 10. Polarization (solid line) and Brightness Temperature (dotted line) Variations from Active Regions 166 and 173 as Observed With the Haystack Antenna at 3.8 cm on 25 February 1971. Plot points are the ratio of observed to a mean value of polarization or temperature. The mean values representative of the entire tracking period are listed on the right side of the figure

26. Straka, R.M., Richards, D.W., and Arora, K.K. (1972) Bull. Am. Astron. Soc. 4:392.

College Park, Maryland. The figure shows two active regions present on the Sun on 25 February 1971 through which a two-line box scan passed through. This allowed the two regions to be alternately sampled once every 72 sec of time. Dotted lines for both regions are the ratios of the region brightness temperatures measured during each scan compared to the mean value of brightness temperature for the whole tracking period. Solid lines are the polarization ratio values compared to the mean. The mean values for Regions 166 and 173 are listed on the right side of the figure as (36,303 °K / -11.9%) and (36,981°K / 9.6%), respectively. Essentially, both regions were about the same intensity. The NOAA Solar-Geophysical Data listed Region 173 as being $\beta\gamma$ in magnetic configuration with a higher 9.1-cm flux density (9 s.f.u.) than Region 166 which had an αp configuration with a 9.1-cm flux density of 7 s.f.u.

Only minor brightness temperature changes were observed at both regions. Of special interest, however, are the rather obvious 10 to 20% variations in polarization for Region 173, which appear to be quiet periodic after 1800 UT with about a 5-min period.

To obtain the power spectra of the polarization variations of these two regions, a simple power series approach was used employing the formulation

$$F(t) = A_o + \sum_{n}^{n=K_{max}} (A_n \cos n\theta + B_n \sin n\theta) ,$$

and

$$P(t) = \sqrt{A^2 + B^2} ,$$

where

$$\theta = \frac{2\pi m}{N} , \quad m = 0 ,$$

N = maximum number of data samples,

K = number of coefficients .

A total of 173 samples for each region were available, spaced 72 sec apart, for a total period of 12,385 seconds. Figure 11 shows the result of this analysis (presented by R. M. Straka at the URSI 1974 Annual Meeting in Boulder, Colorado in a presentation titled "Polarization Variations in Active Regions at 3.8 cm"). The power spectrum for Region 166 (shown as a dashed line) has no significant periodic power components. The spectrum for a quiet-sun control region, shown as the lower solid line also has no periodic components. The reduced power of this spectrum relates to the power scale on the right-hand ordinate.

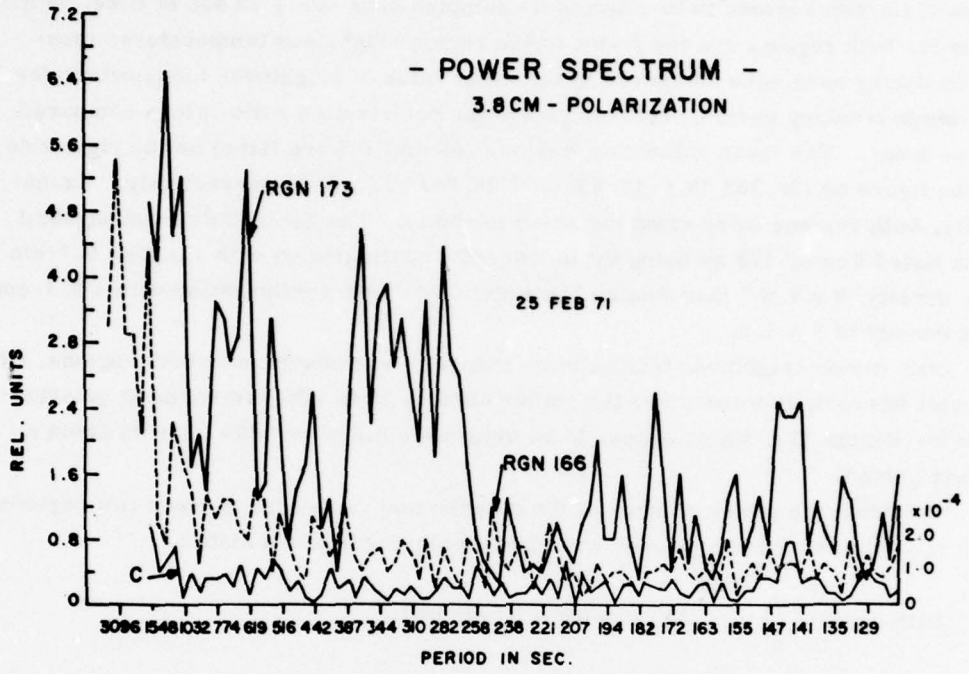

Figure 11. Power Spectra of Regions 173 (top solid line), 166 (dashed line) and a Control Background Sun Position (lower solid line). The ordinate of power values for the control region is on the right side of the figure

Region 173 displayed, on the other hand, a broad component in the 250 to 350-sec period interval. It appears to be a real component. The problem was that numerous other peaks occurred in the periodic power spectrum and, more importantly, there was insufficient data to qualify the significance of the results.

A paper by Sentman and Shawhan,[27] using additional power spectra analysis techniques, questioned the significance of the results of previous radio-periodicity determinations. Using 285 hr of 2-cm wavelength data taken during 1968-1969, they were unable to find statistically significant periodicities in their analysis. This analysis, which was also used to examine the results of others, employed pre-whitening of the data, a Blackman-Tukey algorithm with Hamming smoothing to compute the power spectrum and finally post-darkening of the results. The statistical accuracy of the power spectra was estimated in terms of the degrees of freedom and their associated confidence limits. Their assessment dubbed most studies as having doubtful and marginal reality of results. Only the Durasova et al[25]

27. Sentman, D. D., and Shawhan, S. D. (1974) Solar Phys. 35:83.

periodicity of 280 sec was assessed as real, as well as their own 2-cm wavelength results which had no periodicities. The reason for this latter result undoubtedly can be attributed to the large 1° HPBW they used, where the whole disk was being observed instead of individual active regions. However, due to the questions brought forth by thie report, it was decided to do a more extensive power spectral analysis with the 3.8-cm Haystack data—in particular since there were over 200 hr spent tracking solar active regions in 1973-1974 giving an extended data base.

4.2 Observations

The 120-ft NEROC Haystack radiotelescope tracked active regions with a 4.4-arc min HPBW at 3.8-cm wavelength. Both right and left circular polarizations were monitored simultaneously. Calibration of the system was performed by tracking a quiet region displaced ± 238 millidegrees in declination from the sun center and letting this reference antenna temperature be assigned a value of 100 units. The zero level was established by tracking the background sky level about 20 solar radii from the solar-disk center. Zero percent polarization was assumed for the quiet calibration region, so both the right- and left-circular polarized temperatures were assigned the same value (100). This temperature should equate to a background brightness temperature of about 22,000 °K at 3.8-cm wavelength. Data readouts were obtained once every 3 sec of time (this being an rms average of ten samples digitally sampled once every 0.3 sec) while tracking the active regions; these readouts constituted the time resolutions of the experiment.

4.3 Reduction of Data

Data from each tracking period, which averaged about 1 hr, constituted a data set Y(I), where I = data set index. Typically, a calibration was repeated at the end of each hour, with the tracking resumed for another hour, and so on. The data sets were scanned for suspect points, such as transient interference spikes, that lasted only a sample or two and did not conform to the general solar character of the recorded signal. For the few points that had to be removed, replacement values (obtained by linearly interpolating between the remaining good points) were substituted.

To pre-whiten the data, first differences between the data points were computed such that $y'(i) = y(i + 1) - y(i)$; where $y(i)$ is the original data point and $y'(i)$ is the pre-whitened data point at sample (i). The pre-whitened data forms the set Y2(I). The average value (AVG) and the rms value (rms) were obtained from Y2(I), and the third set Y3(I) was formed such that $Y3(I) = (Y2(I) - AVG) / rms$. This served to normalize the data taken with various tracking periods and for various active regions. To remove large discontinuities between the values of the data

vectors which could produce a Gibbs' ringing phenomenon in the spectrum, the data was tapered at the beginning and end of the data values so that they smoothly approached a mean value of zero. This was accomplished by applying a cosine bell function factor (FACT) to the first and last 1/15th part of the data interval L(i). This tapered data then formed data set Y4(I).

Since one data set exceeded 4096 (2^k, where k = 11) points, all data sets were made 8192 (k = 12) points long by adding zeros to the vector of sample data.

The fast Fourier transform (FFT) was then used on Y4(I) to obtain F(m), where F(O) = O(D. C.) and F(m) = the complex power spectrum ($0 < m \leq 4098$) for frequencies (f), where f = m/3(8192). A Hamming window was then applied to the spectra such that:

$$Y^*(1) = |F(1)|^2 ,$$

$$Y^*(m) = |(0.23\ F(m-1) + 0.54\ F(m) + 0.23\ F(m+1)|^2 ,$$

$$Y^*(4096) = |F(4096)|^2 ,$$

for $1 < m \leq 4096$.

Data sets could then be combined in the frequency domain to obtain:

$$Y(I) = 1/M \sum_{I=1}^{MS} Y^*(I)$$

where Y(I) is the power result, MS is the number of data sets, M is the total number of points (modified for tapering) used in the analysis (summed over all data sets used) and $Y^*(I)$ is the result of all the analysis of the Ith data set shown above. The number of degrees of freedom is approximately M/2048 since (4096 frequencies were analyzed with Hamming).

The power spectrum was also post-darkened in some instances to form $Y_d(I)$ such that:

$$Y_d(i) = Y(I)/2\,(1 - \cos(W^*I))$$

for $1 << I << 4096$,

where $W = \pi/4096$.

4.4 Results

The active region data files were examined and those containing no flare-burst events were submitted to a power spectrum analysis. About 60 hr of data constituted this set. The degrees of freedom for this set was about thirty-four. One degree of freedom is approximately 103 min of data. Figure 12(a) and (b) show these results in two different formats. No outstanding power components of periodicities in polarization are found in (a) for the regions having non-burst activity. The fall-off of the power curve towards the very low frequencies is from the filtering caused by the polynomial to pre-whiten the data which was selected to reduce the low-frequency power. Part (b) has the spectrum plotted in the more familiar post-darkened power form, and shows the low-frequency power. Again, no significant periodicities are evident, with the possible exception of a small component near 1 mHz (1000 sec period).

To determine if pre-flare periodicities occurred in either brightness temperature or polarization, eight files containing flare-bursts were power-spectrum analyzed. This data set had a total of 4.6 hr of preflare data. Figure 13(a) and (b) show the results for the preflare brightness temperature (indicated as TB in the figure), and the polarization (P). Of obvious importance is the strong preflare polarization component at 43 mHz (23 sec period). Not only is it an intense component, but it also is surprisingly narrow in spectral width. No comparable component appears in the brightness temperature spectrum.

As a further test on the validity of this component, the power spectrum was replotted about a normalized level of 1.0 with associated upper and lower 95% confidence limits from a Chi-squared significance test. When the lower confidence level exceeds the normalized value of 1.0 the penplot shows a shaded area to indicate the component is significant to within the 95% confidence level. Figure 14(a) and (b) show the plot with significance levels for the preburst temperature brightness in the frequency intervals 0 to 40 mHz and 40 to 80 mHz. No significant components are present. However, when the polarization plots [Figure 15(a) and (b)] are examined there are indeed some strong components. Besides the expected strong power at the very low frequencies, one notes a significant peak at 4 mHz (250 sec period) which is close to the 280-sec periodicity reported by Durasova et al[25] (which was assessed as statistically real by Sentman and Shawhan).[27]

The Haystack result of the 43 mHz preflare periodicity in polarization (which shows up strongly on Figure 15b) is a new result. It must be remembered that preflare brightness temperature did not show significant periodicities, nor did polarization for the 60 hr of non-burst active region data.

One other test was made with the Haystack data. The temperature and polarization data from the tracked control region were also power analyzed. Figure 16(a) shows the polarization results (the temperature power spectrum results were similar). Since only a short data sample was available the spectrum had large fluctuation levels. As a test of significance the Kolmogoroff-Smirnov probability limit test[28] for white noise was plotted, [see Figure 16(b)]. The inner confidence limits were 75% and the outer limits 90%. From this test, one finds no evidence that the polarization power peaks in Figure 16(a) were not from a white-noise source. Thus, only in the preflare polarization power spectrum were there any significant periodicities detected.

---

28. Jenkins, G. M., and Watts, D. G. (1969) Spectral Analysis and Its Applications, Holde-Day Pub., p. 235.

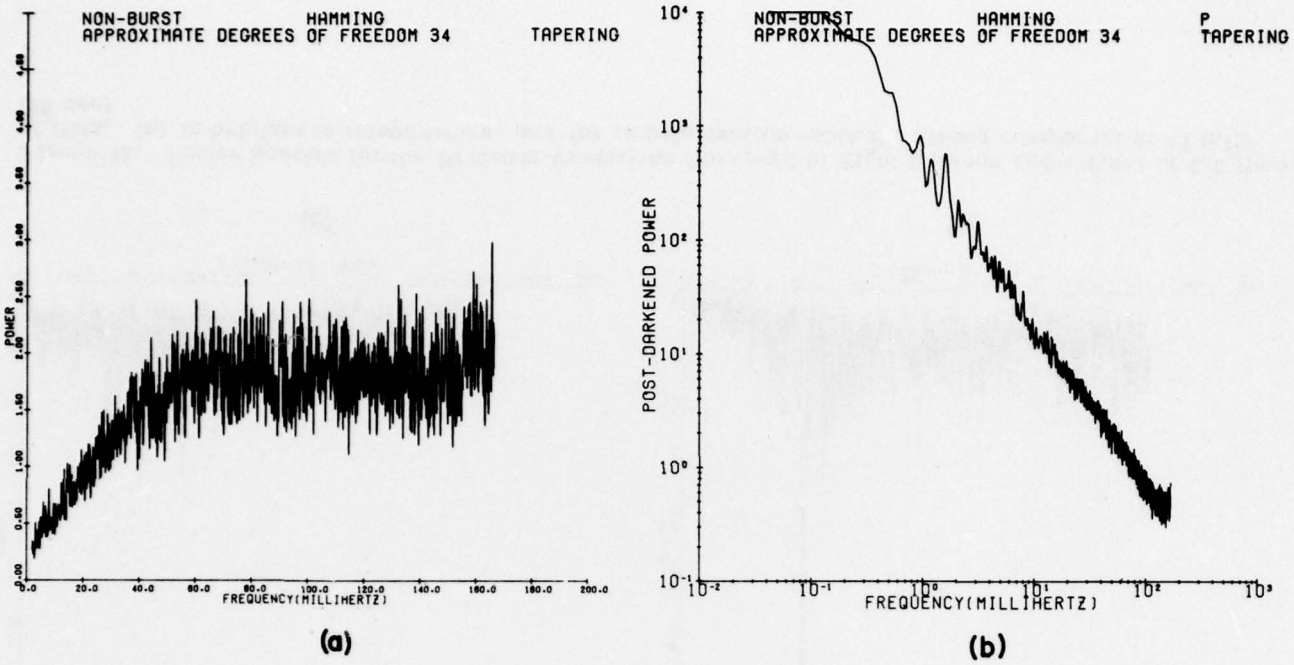

Figure 12. Power Spectra of Polarization Variations in Non-burst Producing Active Regions. About 60 hours of data for these regions was obtained during 1973-1974. (a) Linear plot of power spectrum, and (b) logarithmic plot with post-darked power

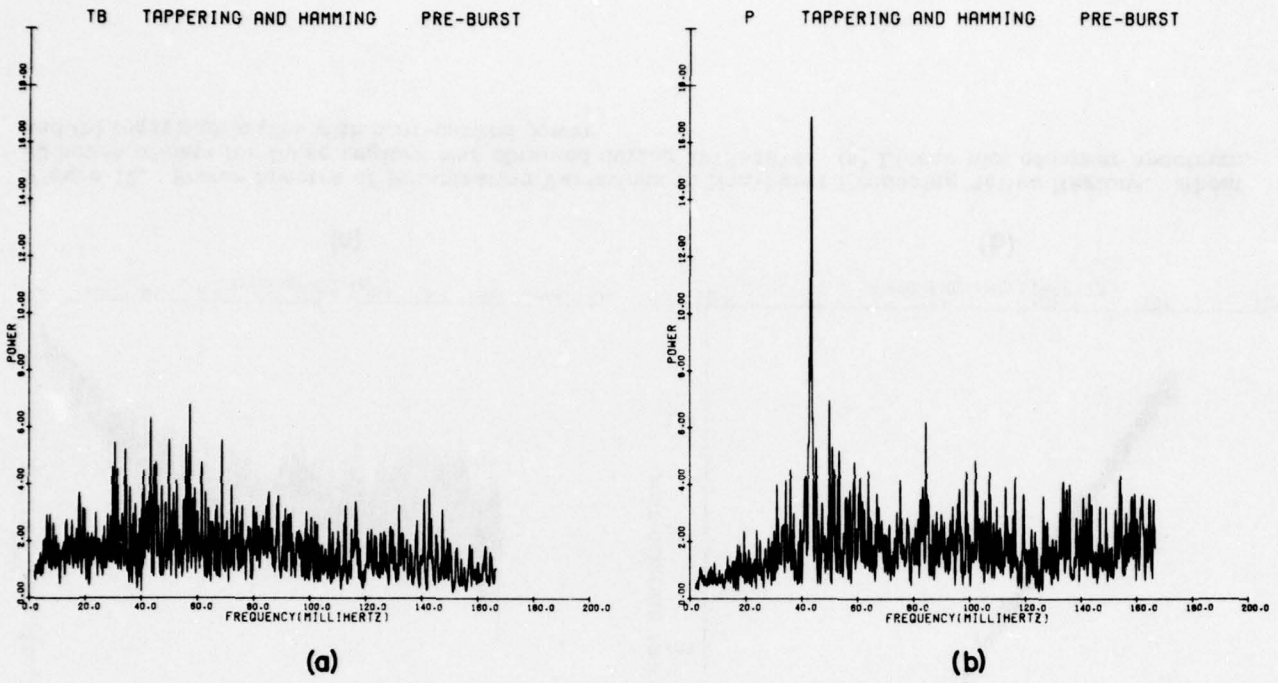

Figure 13. Power Spectra for the Preburst Variations Observed in Eight Regions and a Total of 4.6 Hours of Data. (a) In brightness temperature, and (b) in polarization—note the strong component at 43 mHz (23 sec)

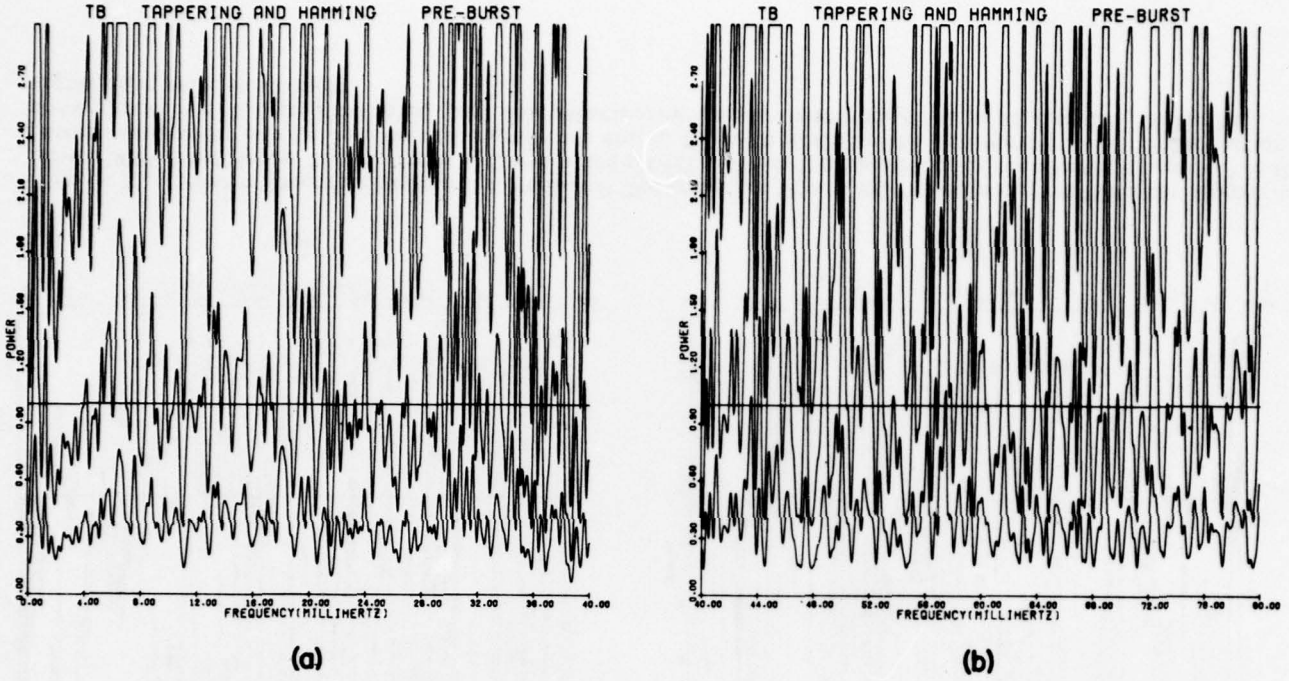

Figure 14. Power Spectra Showing the Preburst Brightness Temperature Spectrum (middle curve) With the Upper and Lower 95% Confidence Limits from a Chi-squared Test. When the lower confidence level exceeds 1.0 the power component can be considered significant and is filled in solid by the pen plotter. Note the lack of significant components for temperature. (a) Brightness temperature power spectrum 0.0 to 40.0 mHz, and (b) brightness temperature power spectrum 40.0 to 80.0 mHz

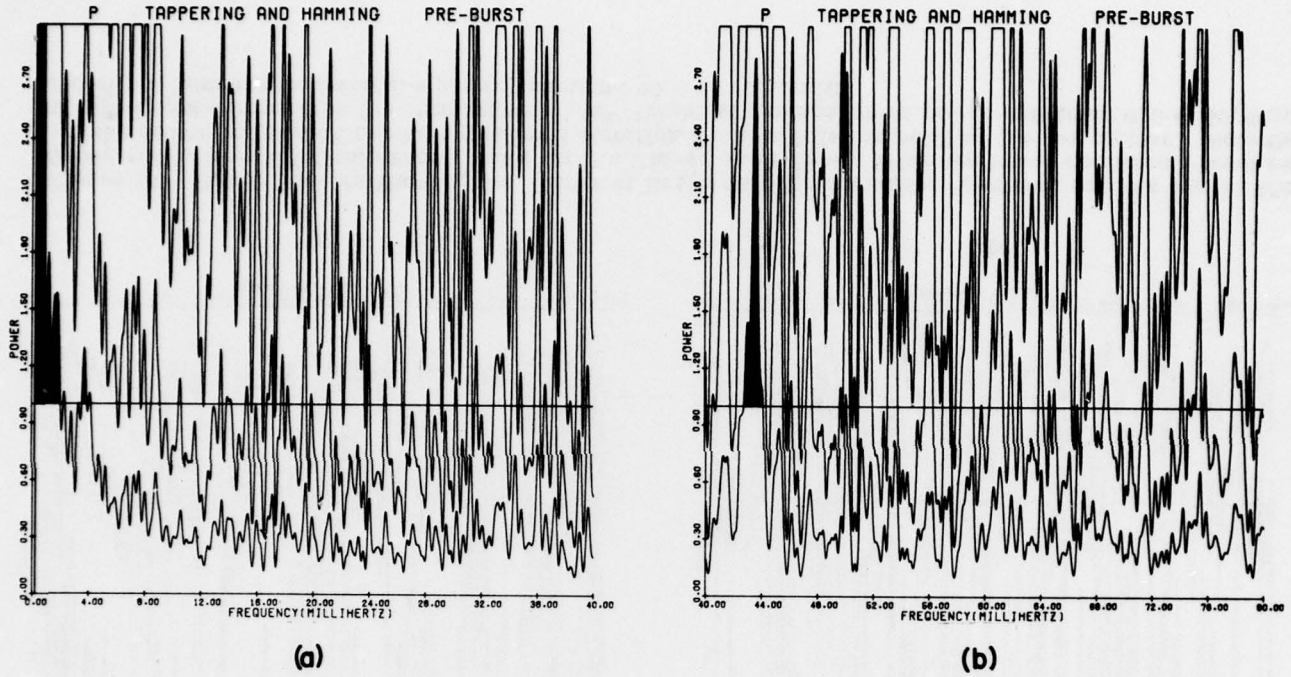

Figure 15. Power Spectra Showing the Preburst Polarization Spectrum (middle curve) With the Upper and Lower 95% Confidence Limits from a Chi-squared Test. When the lower confidence level exceeds 1.0 the power component can be considered significant and is filled in solid by the pen plotter. (a) Polarization power spectrum 0.0 to 40.0 mHz, and (b) polarization power spectrum 40.0 to 80.0 mHz. Note the significant peak at 43 mHz

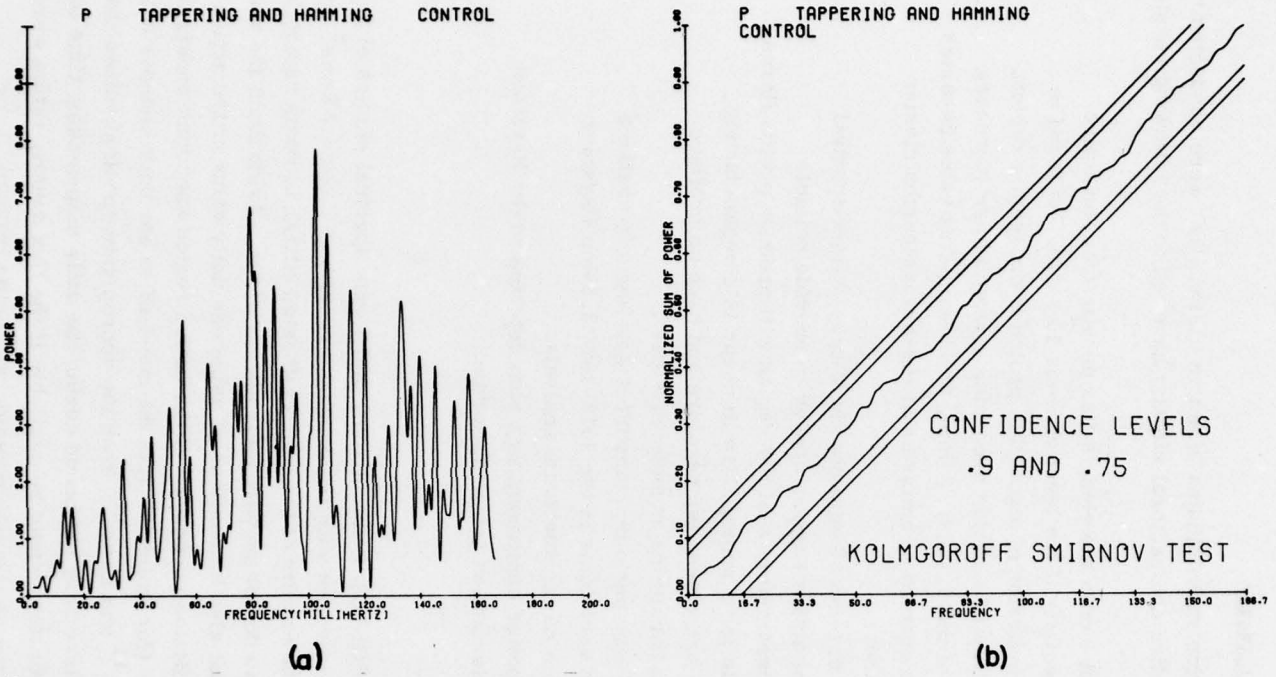

(a) (b)

Figure 16. Temperature and Polarization Data From Quiet-Sun Background. (a) Power spectrum from the control region of quiet Sun background, and (b) Kolmogoroff-Smirnov significance test of the polarization components from the control region. The outer lines are the 90% confidence limits, and the inner at 75% limits

5. HIGH RESOLUTION STUDIES CONCLUSIONS

5.1 In-House Work Unit 46430302

The high resolution radio studies of active regions that were conducted under this work unit (excluding contractoral efforts) have led to the following results and conclusions:

(1) The apparent 3-mm wavelength flux density from an active region, especially if the level exceeds 10 s.f.u., is found to be the best indicator of a possible proton event from a region,

(2) The probability of a region producing a proton flare increases as the sum of the 9.1-cm, 8-mm, and 3-mm-flux value becomes high and the centers of emission at these wavelengths cluster closer together,

(3) Neither the 9.1-cm / 8-mm nor the 8-mm / 3-mm spectral indices from active regions appear to provide reliable prediction parameters that the region will produce proton flares,

(4) It is possible for a proton flare to occur in a region having low 3.8-cm brightness temperature and have no preflare polarization variations associated with it,

(5) A strong 23-sec periodic component was found in preflare polarization variations in the 1973-1974 3.8-cm Haystack active-region power spectrum analysis,

(6) A 250-sec power component was also detected in the Haystack preflare polarization power spectrum.

5.2 Discussions

The result of AFGL's 9.1-cm, 8-mm, and 3-mm spectral studies of active regions appears not to agree with the Japanese results at 7.5-cm / 3-cm[8] and 3-cm / 1.8-cm[9]. The results of the well-calibrated NELC LaPosta radiotelescope at 2-cm / 8-mm[5] also do not support their observations. Aside from the wavelength differences, one must also be cautious of using one daily value of the active region flux density for prediction purposes. If the active region spectrum undergoes short time-period changes (for example, like the one-half to one hour changes noted by Richards and Straka[11] and Lang[12]), then the appropriate spectral values that forewarn of the proton flare may not occur during the daily map-making time interval. A more effective indication would be available if the flux density ratios were monitored in real-time as the active region was being tracked.

One area which this in-house study did not pursue, but which appears promising for long term forecasting of proton regions, is the one associated with the

polarization configuration of the active region prior to a proton flare. Enome and Tanaka[29] found that a requirement for a region to have a proton flare was that the 3-cm circular polarization had to have a special distribution in the source such that there was a strongly polarized main peak and subpeaks on either side that are oppositely polarized. They called this the P-configuration. Optical observers often have noted similar magnetic configurations in regions that had proton flares.

The Haystack results with the 21 August 1975 proton flare point out the problems of using too large a beamwidth radiotelescope, in particular for regions near the solar limbs. Although the chance of detecting an event from an unsuspected region (for example, McMath 13811) is reduced, a more detailed physical picture can be constructed of the region of flaring with the higher resolution solar radio instruments. More support should be given to future studies with the large radiotelescopes to study the small very hot and polarized sources that may be associated with the flare trigger mechanism, and which so far appear to give advance indication of flare activity.

An important potential preflare indicator has been presented in this report, that of the 23-sec periodicity in polarization. If, with more observations, confirmation of these results are obtained, one could conceive of a 3-cm system performing a real-time spectral analysis looking for the 23 sec period with a pass band filter, and triggering an alert for flare activity if the component was detected.

Recent results by Kobrin et al[30] indicate that long periodicities, 30 to 80 min, in the 3-cm wavelength range may provide long-term predictors of proton events. They find that, several days prior to the flare, well-defined fluctuations of the slope of the spectrum between 9870 and 9670 MHz with periods 30 to 80 min began to be observed.

Many of the results reported herein, however, suffer from the lack of sufficient data to obtain statistically significant results. Unfortunately, the new very-high-resolution radiotelescope instrumentation and power spectrum analysis of the data came at a time of low activity in the solar 11-year cycle. Now, however, as the solar activity increases, it is vitally important to explore these partially-proven radio techniques for the payoff they promise as operationally-useful predictors of proton-flare activity.

---

29. Enome, S., and Tanaka, H. (1973) High Energy Phenomena on the Sun Symposium Proceedings, ed. R. Ramaty and R. G. Stone, p 78.

30. Kobrin, M. M., Korshunov, A. I., Arbuzov, S. I., Pakhomov, V. V., and Fridman, V. M. (1976) Sov. Astron. 20:444.

5.3 Recommendations

(1) Tracking of active regions should be performed simultaneously at several wavelengths with a real-time readout of the spectral flux density ratios to determine the time-dependent character of proton producing regions.

(2) More very high spatial and time resolution studies of the small highly-polarized bright sources that appear before flares should be made to determine their role as possible flare-trigger contributors.

(3) Confirmation should be sought of the 43 mHz (23 sec period) preflare polarization periodicity and the long period (30 to 80 min) spectrum fluctuations to establish their significance as flare/proton flare predictors.

References

1. Kundu, M.K. (1965) Solar Radio Astronomy, Interscience Publishers, New York, p 168.
2. Kundu, M.K. (1959) Ann. Astrophys. 22:1.
3. Simon, Michael (1965) Astrophys. J. 141:1513.
4. Mayfield, E.B., Higman, J.A., and Samson, C.F. (1970) Solar Phys. 13:372.
5. Bleiweiss, M.P., Wefer, F.L., and Hurst, M.D. (1976) NELC Technical Note TN-3262.
6. White, K.P. III (1972) Aerospace Rpt. No. ATR-73(8102)-4.
7. Withbroe, G.L., and Vernazza, J.E. (1976) Solar Phys. 50:127.
8. Tanaka, H., and Kakinuma, T. (1964) Rpt. on Iono. and Space Res. in Japan 18:32.
9. Nakajima, H. (1973) Rpt. on Iono. and Space Res. in Japan 27:149.
10. Gelfreykh, G.B., Derevyanko, O.G., Korzhavin, A.N., and Stasyuk, N.P. (1970) AFCRL-70-0490 Translation No. 69.
11. Richards, D.W., and Straka, R.M. (1971) Nature - Phys. Sci. 233:92.
12. Lang, K.L. (1974) Solar Phys. 36:351.
13. Svestka, Z., and Simon, P. (1975) Catalog of Solar particle Events 1955-1969 D. Reidel Publ. Co., Dordrecht Holland/Boston USA.
14. Smart, D., and Shea, P. (1976) Private Communications.
15. Straka, R.M., and Barron, W.R. (1970) AGARD Proc. of Symposium on Ionospheric Forecasting 49:10-1.
16. Dodson, W.H., and Hedemen, E.R. (1967) Structure and Development of Solar Active Regions, I.A.U. Symposium No. 35, ed. K.O. Kiepenheuer, D. Reidel Publ. Co., Dordrecht, Holland.
17. Bleiweiss, M.P., Wefer, F.L., and Hurst, M.D. (1976) NELC Tech Rpt. TR-1999.

18. Castelli, J.P., Aarons, J., and Michael, G.A. (1967) J. Geophys. Res. 72:5491.

19. Papagiannis, M.D., and Kogut, J.A. (1975) AFCRL Tech. Rept. TR-75-0430.

20. Lang, K.R. (1977) Solar Phys. 52:63.

21. Noyes, R.W. (1967) Proc. I.A.U. Symp. No. 28, 293.

22. Simon, M., and Shimabukuro, F.I. (1971) Astrophys. J. 168:525.

23. Lang, K.L. (1974) Astrophys. J. 192:777.

24. Yudin, O.I. (1968) Soviet Phys. Doklady 13:503.

25. Dursova, M.S., Dobrin, M.M., and Yudin, O.I. (1971) Nature 229:82.

26. Straka, R.M., Richards, D.W., and Arora, K.K. (1972) Bull. Am. Astron. Soc. 4:392.

27. Sentman, D.D., and Shawhan, S.D. (1974) Solar Phys. 35:83.

28. Jenkins, G.M., and Watts, D.G. (1969) Spectral Analysis and Its Applications, Holde-Day Pub., p 235.

29. Enome, S., and Tanaka, H. (1973) High Energy Phenomena on the Sun Symposium Proceedings, ed. R. Ramaty and R.G. Stone, p 78.

30. Kobrin, M.M., Korshunov, A.I., Arbuzov, S.I., Pakhomov, V.V., and Fridman, V.M. (1976) Sov. Astron. 20:444.